Environmental Science & Technology

pubs.acs.org/est

Article

# Mineral Scale Prevention on Electrically Conducting Membrane Distillation Membranes Using Induced Electrophoretic Mixing

Unnati Rao, Arpita Iddya, Bongyeon Jung, Chia Miang Khor, Zachary Hendren, Craig Turchi, Tzahi Cath, Eric M. V. Hoek, Guy Z. Ramon, and David Jassby*

Cite This: https://dx.doi.org/10.1021/acs.est.9b07806

Read Online



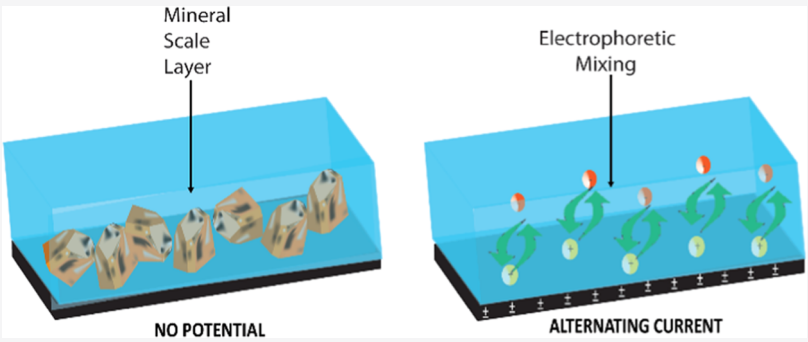


**ABSTRACT:** The growth of mineral crystals on surfaces is a challenge across multiple industrial processes. Membrane-based desalination processes, in particular, are plagued by crystal growth (known as scaling), which restricts the flow of water through the membrane, can cause membrane wetting in membrane distillation, and can lead to the physical destruction of the membrane material. Scaling occurs when supersaturated conditions develop along the membrane surface due to the passage of water through the membrane, a process known as concentration polarization. To reduce scaling, concentration polarization is minimized by encouraging turbulent conditions and by reducing the amount of water recovered from the saline feed. In addition, antiscaling chemicals can be used to reduce the availability of cations. Here, we report on an energy-efficient electrophoretic mixing method capable of nearly eliminating $CaSO_4$ and silicate scaling on electrically conducting membrane distillation (ECMD) membranes. The ECMD membrane material is composed of a percolating layer of carbon nanotubes deposited on porous polypropylene support and cross-linked by poly(vinyl alcohol). The application of low alternating potentials (2 $V_{pp,1Hz}$) had a dramatic impact on scale formation, with the impact highly dependent on the frequency of the applied signal, and in the case of silicate, on the pH of the solution.



## 1. INTRODUCTION

Membrane-based desalination technologies have been demonstrated to be the most energy-efficient methods to produce fresh water from saltwater. Membrane distillation (MD) is a membrane-based thermal desalination technology that has the potential to become a mainstream process for the treatment of high-salinity brines (e.g., oil and gas wastewater), particularly when free thermal energy is available (e.g., from geothermal brines).[1,2] While nanofiltration (NF) and reverse osmosis (RO) are by far the most common membrane-based desalination methods, these membranes are not capable of effectively treating high-salinity brines (>70 g $L^{-1}$), due to the excessive hydraulic pressure needed to overcome the solution's osmotic pressure. In fact, the treatment of high-salinity brines is a growing challenge across multiple regions and industries, and MD has shown great treatment potential due to its high efficiency, excellent performance, and low capital costs.[3,4]

In the MD process, a high-salinity feed stream is heated and passed along the surface of a microporous hydrophobic membrane that separates the hot liquid feed from the desalinated cool permeate. A partial vapor pressure difference (generated by the temperature difference between the feed and the permeate) leads to water vapor diffusing across the membrane's hydrophobic pores, which then condense in the permeate channel, leaving concentrated dissolved constituents (e.g., ions, particles, and pathogens) on the feed side of the membrane.[3,5] Operating the MD system below the membrane's liquid entry pressure ensures that liquid feed water

Received: December 22, 2019
Revised: January 22, 2020
Accepted: February 24, 2020
Published: February 24, 2020

(carrying salt and other contaminants) does not penetrate into the permeate stream.[6,7] MD systems can be operated using different configurations, including "direct contact" (DCMD), "air gap", "sweeping gas", and "vacuum". Electrically conducting MD membranes (ECMD), fabricated through the deposition of a percolating network of carbon nanotubes (CNTs) onto a hydrophobic porous substrate, have higher water flux, self-heating capability, and self-cleaning properties.[2,8] In addition, other electrically conducting membranes have been shown to have multiple antifouling properties[3,6,9] and have the potential of substantially improving many membrane-based treatment processes.

All membrane-based desalination technologies (and indeed, many other industrially important surfaces, such as heat exchangers) experience multiple forms of surface fouling. In desalination membranes, the passage of pure water through the membrane leads to the formation of a stagnant concentration polarization (CP) layer along the membrane surface.[8,10] In this layer, the concentration of ions can exceed the solubility limit of certain sparingly soluble salts, which can form a deposit layer on the membrane surface, known as the mineral scale.[11−13] Mineral scaling blocks the membrane's pores, which restricts the passage of water (either liquid or vapor) and can physically damage the membrane's fragile structure.[14] Due to the porous structure of MD membranes, the mineral scale can grow inside the membrane's pores, which can lead to membrane wetting (i.e., the formation of hydrophilic pathways through the hydrophobic structure of the membrane) and process failure.[15] The conditions controlling the formation of mineral scale vary widely and depend on feed water chemistry (pH, dissolved species), feed physical conditions (temperature, mixing), and membrane surface properties (roughness, charge, and hydrophilicity).[16,17] The degree of water recovery (i.e., % of the feed water volume that becomes product water) in desalination is largely controlled by fouling, with mineral scaling being the primary limitation of achieving high recoveries in groundwater desalination because groundwater contains many multivalent ions that tend to form sparingly soluble minerals (e.g., $CaSO_4$, $CaCO_3$, and $(SiO_{4-x}{}^{(4-2x)-})_n$).[18] There is a strong environmental and economic incentive to increase water recovery during desalination, as this reduces the volume of waste brine that requires disposal.[19] In fact, mineral scaling impacts other industrial processes, notably heat exchangers, which reduces their efficiency due to the buildup of poorly conducting layers on the exchanger surface.[20,21] Thus, there is a need to develop new materials and processes that minimize the formation or deposition of the mineral scale at the solid/liquid interface.

The precipitation of minerals from solution can occur via a homogeneous (slow) or heterogeneous (fast) precipitation process.[22,23] The conditions inside a membrane desalination system favor heterogeneous precipitation, due to the presence of a solid/liquid interface (i.e., the membrane/feed stream), which can lead to rapid membrane scaling.[24] During the heterogeneous precipitation process, it is thought that amorphous mineral "prenucleation clusters", numbering just a few atoms, rapidly (within seconds) form in the bulk in areas with the highest concentration (e.g., at the membrane/water interface).[25] These clusters can aggregate and attach to a surface and serve as induction sites (nuclei) for crystal growth on the surface, where the nuclei grow due to the addition of dissolved ions from the liquid phase, assuming a crystalline structure as their size increases.[26,27] This results in surface scale formation due to heterogeneous crystallization. Thus, to prevent the formation of the mineral scale, an ideal system would minimize the formation of these prenucleation clusters, prevent any of these clusters from reaching the membrane surface, and limit subsequent growth of a surface crystal structure. Many studies have investigated the kinetics of mineral scale formation during membrane desalination.[28,29] These studies determined that the rate of scale formation is highly dependent on the degree of supersaturation, with the period of time between the onset of supersaturation and the formation of mineral scaling defined as the "induction period."[30,31]

The surface charge on a membrane surface has been demonstrated to impact the formation of the mineral scale, with negatively charged surfaces (e.g., rich in −COOH groups) being more scaling resistant than positively charged surfaces (e.g., rich in quaternary amine groups).[32,33] However, when a direct current (DC) external anodic potential (1.5 V cell potential) was applied to the surface of an electrically conducting RO membrane, $CaSO_4$ scaling was significantly delayed. The antiscaling phenomena were explained through the formation of a thick electrical double layer (EDL), which developed in response to the applied potential.[34] In the EDL, the concentrations of co-ions are depleted relative to those of counter ions, which reduces the formation of crystal nuclei by locally lowering the saturation index and slows down mineral scaling. Importantly, these results suggest that external control of ion concentrations along a surface can substantially impact the rate of nucleation and potentially prevent mineral scaling.

In this study, we report on an efficient antiscaling method employing alternating currents (AC) applied to the surface of ECMD membranes. The method is applied to prevent both gypsum ($CaSO_4$) and silicate scaling, which are common scaling species encountered during groundwater desalination. We hypothesize that the application of an AC potential at an appropriate frequency induces electrophoretic mixing of the stagnant CP layer, which minimizes the formation of prenucleation clusters and prevents the formation of the mineral scale. The results presented in this study are relevant to other membrane-based desalination processes and potentially to other surfaces experiencing mineral scaling, such as heat exchangers. These findings can be potentially applicable to other common scaling species, such as $CaCO_3$ and iron oxide.

## 2. MATERIALS AND METHODS

**2.1. Chemicals.** Sodium sulfate ($Na_2SO_4$), magnesium sulfate ($MgSO_4$), sodium metasilicate pentahydrate ($Na_2SiO_3 \cdot 5H_2O$), aluminum chloride hexahydrate ($AlCl_3 \cdot 6H_2O$), barium chloride dihydrate ($BaCl_2 \cdot 2H_2O$), ferric chloride hexahydrate ($FeCl_3 \cdot 6H_2O$), calcium chloride dihydrate ($CaCl_2$), potassium chloride (KCl), and magnesium chloride hexahydrate ($MgCl_2 \cdot 6H_2O$) were purchased from Sigma-Aldrich and used as received to prepare the feed solutions. Sodium dodecylbenzene sulfonate (Na-DDBS), poly(vinyl alcohol) (PVA), glutaraldehyde (GA), and hydrochloric acid (HCl) were purchased from Sigma-Aldrich and used as received to prepare the membrane materials. COOH-functionalized multiwalled CNTs were purchased from Cheaptubes (Cheaptubes inc., Brattleboro, VT). The CNTs are reported to have an outer diameter of 13−18 nm, a length of 1−12 $\mu$m, and purity ≥99% with a functional group content of 7.0 ± 1.5%.

**2.2. Scaling Solution.** Two different feed water solutions were used to evaluate membrane scaling. The first solution


https://dx.doi.org/10.1021/acs.est.9b07806
Environ. Sci. Technol. XXXX, XXX, XXX−XXX

simulates brackish groundwater from the California Buena Vista Water Storage District (Table S1) and was unsaturated with respect to all of the ions at a temperature of 90 °C (water temperature in feed tank during the MD process). The saturation index (SI) (calculated using visual MINTEQ version 3.1) with respect to $CaSO_4$ (gypsum) was determined to be 0.59, suggesting that $CaSO_4$ formation is not thermodynamically preferable in the bulk solution.[35] The SI was calculated using eq 1

$$\mathrm{SI} = \left( \frac{[\mathrm{Ca}^{2+}][\mathrm{SO4}^{2-}]}{K_{\mathrm{sp,CaSO_4}}} \right) \tag{1}$$

A feed solution prone to silicate scaling, simulating a geothermal brine from Nevada, was used as the second feed (Table S2). However, to speed up the scaling process, the concentration of salts was increased by a factor of 6. The saturation indices of the different potential insoluble salt species in this solution are presented in Figure S1. While the feed solution has multiple potential insoluble species (SI > 0), the most likely species to form sufficient deposits to obstruct flow (and reduce flux) are dominated by silicate species due to their far higher concentrations (Figure S1). The SI of silicate species in the feed was just below 0, indicating that precipitation of these species in the feed solution was not likely.

**2.3. Fabrication of ECMD Membranes.** Polypropylene (PP) membranes with a nominal pore size of 0.59 $\mu$m and thickness of 110 $\mu$m (3M, Charlotte, NC) were used as the substrate for the fabrication of ECMD membranes. These substrates were coated with a CNT ink via a spray-coating process.[36] To prepare the CNT ink, a 1 g $L^{-1}$ CNT solution was prepared by dispersing the CNTs (1 g) in water (1000 mL) along with the surfactant Na-DDBS (10 g) using an ultrasonic horn sonicator (Branson, Danbury, CT).[37] The suspension was sonicated for 30 min, followed by centrifuging (Beckman Coulter, Brea, CA) for 20 min at a speed of 11 000 rpm. A 0.1% solution of PVA was prepared by stirring and heating a solution of PVA (1 mL) in water (100 mL) to 95−100 °C for 1 h and then diluting it by a factor of 10. CNT ink (200 mL) followed by PVA solution (2 mL) was spray-coated in a layer-by-layer manner using a custom-built spray coater onto a 16 cm × 30 cm piece of the PP substrate. The surfactant was then washed away by rinsing the membrane with a steady flow of deionized (DI) water for 2 h. The CNT/PVA network was cross-linked by soaking the material in the crosslinking solution at 70 °C for 1 h. The crosslinking solution was prepared by dissolving HCl (10 mL) and GA (10 mL) in water (1000 mL). Following this, the membrane was rinsed in deionized water and air-dried. The membrane was then used for testing without any further modification.

**2.4. System Design and Operation.** Membrane performance was tested using a polycarbonate flow cell housing an MD membrane in a flat-sheet configuration and operated in DCMD mode (Figure S2). The flow channels on either side of the membrane (feed and permeate) were 8 cm × 5 cm, with a height of 4 mm. Temperature-resistant tubing, insulated using ultra-high-temperature mineral wool insulation (McMaster-Carr, Santa Fe Springs, CA), was used to circulate the feed and permeate solutions. The feed was placed in a 10 L tank (McMaster-Carr, Santa Fe Springs, CA) placed on a stir plate (Fisher Scientific, Hampton, NH) and heated with an immersion heater (Process Technology, VXIIII, Mentor, OH) while stirring at 250 rpm. Five temperature sensors (Vtech, DS18b20) were placed throughout the system: one in the feed tank, and one at each of the flow cell inlets and outlets (Figure S2). The temperature sensors were connected to a temperature control unit, and the temperature of the hot feed solution could be maintained at a constant value using a PID cascade loop. A vertically mounted level float switch (Madison, M8000, Branford, CT) was used to maintain the liquid level in the feed tank by recirculating it from a permeate buffer tank; this ensured the feed solution was kept at a constant concentration and SI. This was done to ensure no bulk precipitation occurred in the feed tank, which could deposit on the membrane and lead to flux decline. A peristaltic pump (Cole Parmer, Pump Drive Model 7553-70, Pump Head Model 77200-50, Vernon Hills, IL) was used to circulate the feed solution, and gear pumps (Greylor, PQ-12/24, Cape Coral, FL) were used for the permeate and the buffer tank. The permeate was collected in a plastic tank placed on a balance (Fisher Scientific Education Precision Balance, Hampton, NH), with cold water continuously circulated on the permeate side; permeate temperature was maintained at 20 °C using a chiller (6500 Series, 1/2 HP, Polyscience, Niles, IL). A conductivity meter (Thermo Scientific, Orion Star A322, Waltham, MA) was placed in the permeate tank to monitor changes in salt concentration (and thus salt rejection and membrane wetting). The system was operated and controlled using the open-source hardware (Arduino) and software (Python).[38] Flux through the membrane was measured by the change in weight of the permeate tank. The cross-flow velocities of the feed and permeate solutions were maintained at 8 cm $s^{-1}$, resulting in Reynold's number of 215. While the temperature in the feed tank was maintained at 90 °C, there was a 12 °C temperature drop from the feed tank to the flow cell inlet, resulting in an inlet temperature of 78 °C. A plastic mesh was used as a spacer on the permeate side, but no spacer was used on the feed side (to encourage scaling). All experiments were conducted in triplicate, with averages and 95% confidence intervals reported.

To connect the membrane to an external potential source, the membrane surface was coupled to an electrode (a stainless-steel machine key stock placed outside of the O-ring, so the electrode does not come in contact with the feed stream), and a Pt-coated Ti sheet served as the counter electrode and placed 3 mm above the membrane surface inside the feed channel. An arbitrary waveform generator (Rigol, Beijing, China) was used to provide the electrical potential to the membrane/counter electrode. During the experiments, different electrical conditions were imposed on the membrane/counter electrodes while maintaining all other operating conditions constant (feed and permeate flow rates and temperatures). To modify the pH during one set of experiments, HCl was added to the feed solution until a pH of 6 was reached.

**2.5. Membrane Characterization.** Membrane surfaces were analyzed using scanning electron microscopy (SEM) (Zeiss Supra 40 VP, Carl Zeiss Microscopy, LLC, NY). Samples were secured on SEM stubs using double-sided carbon tape and sputter-coated (Ion beam sputtering/etching system, South Bay Technology, San Clemente, CA) with iridium before imaging. Quantitative analysis and surface elemental mapping were carried out using energy-dispersive X-ray spectroscopy (EDAX), which is a module included with the Zeiss Supra SEM. Crystal structures deposited on the membrane surface were studied using X-ray diffraction


https://dx.doi.org/10.1021/acs.est.9b07806
Environ. Sci. Technol. XXXX, XXX, XXX−XXX

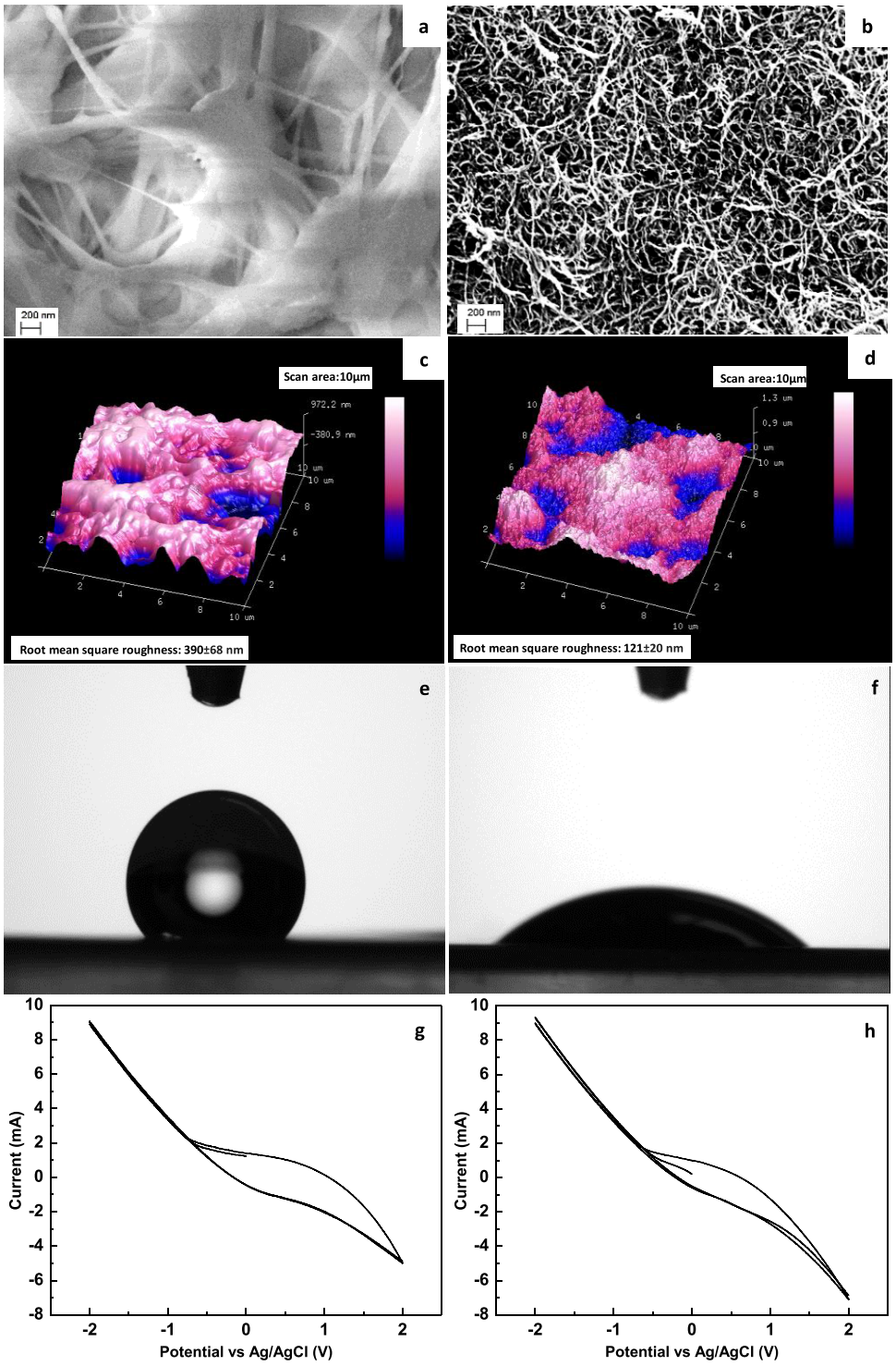


**Figure 1.** Surface and electrochemical properties: SEM micrographs of (a) the bare PP membrane and (b) the ECMD membrane; AFM micrographs of (c) the bare PP membrane and (d) the ECMD membrane; water contact angles of (e) the bare PP membrane and (f) the ECMD membrane; CV curves of the ECMD membrane as the working electrode in (g) $CaSO_4$ feed solution and in (h) silicate feed solution.

(XRD: Panalytical X'Pert Pro). The scaled membrane was placed in the sample holder for analysis. The ordinary method for XRD analysis is by scraping off the powder and putting it in the sample holder. However, we could not recover sufficient (2 g) powder for this and had to use the scaled membrane directly in the sample holder. Current was measured using a digital multimeter (Mastech, MS8268, Pittsburgh, PA). Surface roughness was determined using a Bruker Dimension FastScan Scanning Probe Microscope (Bruker, Billerica, MA). Membrane sheet resistance was measured using a 4-point conductivity probe (Mitsubishi, MCP-T610, Tokyo, Japan). Contact angle measurements were conducted using a contact angle goniometer (Rame-Hart, Model 250, Netcong, NJ). Electrochemical impedance spectroscopy (EIS), cyclic voltammetry (CV), open circuit potential (OCP), and current response measurements were carried out using a potentiostat


https://dx.doi.org/10.1021/acs.est.9b07806
Environ. Sci. Technol. XXXX, XXX, XXX−XXX

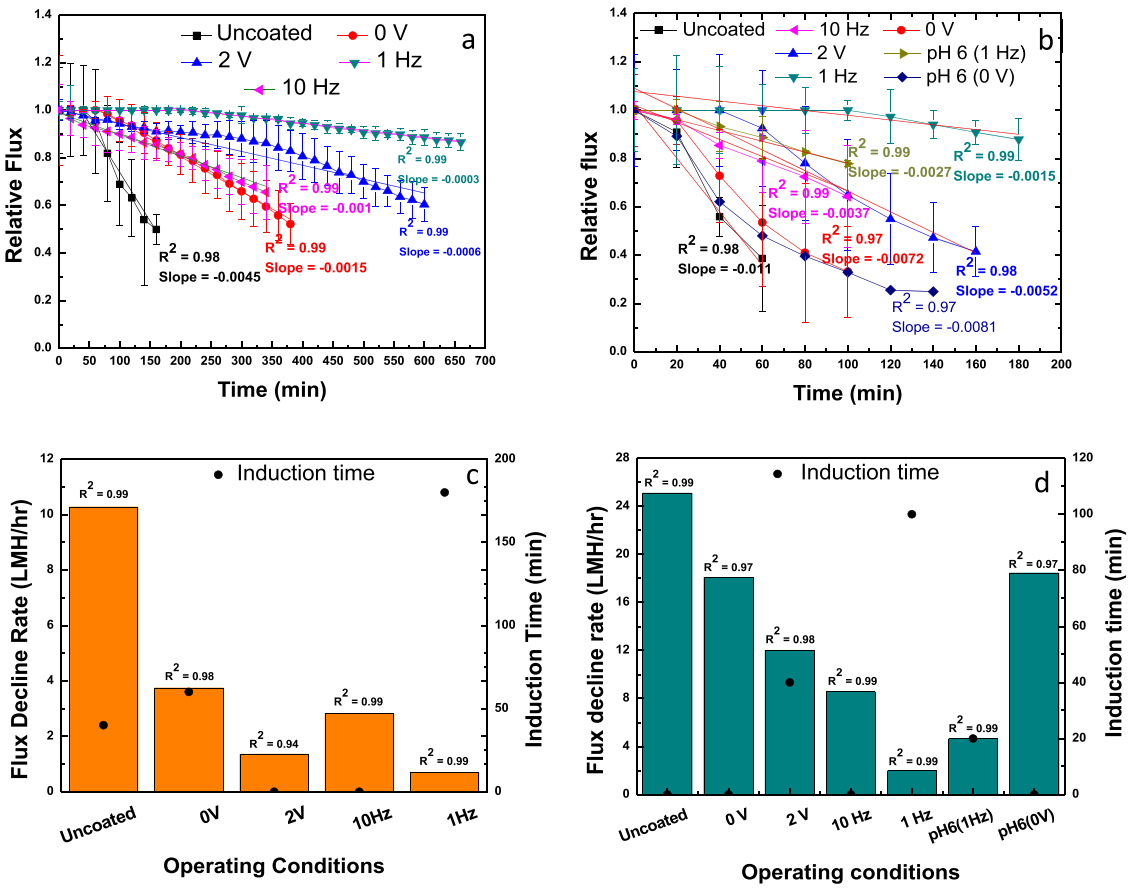


**Figure 2.** Flux decline under different applied electrical conditions with (a) $CaSO_4$ and (b) silicate solutions as the feed. The rate of flux decline under different conditions for (c) $CaSO_4$ and (d) silicate solutions.

(CH Instruments, Austin, TX) with a Ag/AgCl reference electrode. In these experiments, the feed solution was placed in a stirred (250 rpm) beaker with the two electrodes (the ECMD membrane as the working electrode and Pt-coated Ti as the counter electrode) separated by 4 cm to allow for the placement of the Ag/AgCl reference electrode. EIS tests were carried out over a frequency range between 0.1 and 100 Hz with an amplitude of 5 mV (10 $mV_{pp}$). Cyclic voltammetry measurements were conducted over a range of −2 V to +2 V. Open circuit potential measurements were conducted at −2 V, and current response measurements were carried out under conditions of 2 $V_{DC}$ and 2 $V_{AC,1Hz}$.

## 3. RESULTS AND DISCUSSION

**3.1. Membrane Characterization.** The pure water flux for an uncoated PP membrane with a feed temperature of 78 °C and cross-flow velocity of 8 cm $s^{-1}$ was determined to be 39.2 ± 3.3 L $m^{-2}$ $h^{-1}$ (LMH). However, the flux for the CNT/PVA membrane composite was 51.7 ± 2.9 LMH, a 32% increase. This increased flux is consistent with previous reports that describe a significant flux enhancement when hydrophobic support is coated with a hydrophilic CNT layer, although the mechanism behind this enhancement is unclear. When 2 $V_{DC}$ was applied, the steady-state pure water flux was similar (49.1 ± 1.3 LMH), indicating that applied potential has no significant effect on pure water flux through the CNT-coated membrane. SEM micrographs of the membrane surface (both the bare PP substrate and the CNT/PVA-coated substrate) can be seen in Figure 1a,b. While the addition of the CNT/PVA layer added an additional barrier to water transport, formed by the nonwoven mesh-like structure of the deposited CNTs with an average pore size of 100 nm, the membrane's performance was still enhanced (in terms of flux). The analysis of a cross-sectional image of the CNT/PVA-coated membrane shows that the thickness of this layer was 2 $\mu$m (not shown). AFM was used to determine the surface roughness of the bare PP and the CNT/PVA composite materials, with the root mean squares of roughness found to be 390 ± 68 and 121 ± 20 nm, respectively (Figure 1c,d). The membrane's sheet resistance was determined to be 228 ± 14 Ω/square, which translates into a conductivity of approximately 2200 S $m^{-1}$. The contact angles of the bare PP membrane and the CNT/PVA-coated membrane were determined to be 135.5 ± 0.8 and 39.7 ± 0.3°, respectively (Figure 1e,f). CV curves show the onset of water electrolysis at 0.9 and −0.7 V vs Ag/AgCl, for anodic and cathodic conditions, respectively, in the $CaSO_4$ scaling solution (Figure 1g). In the silicate solution, water electrolysis occurred at 1 and −0.55 V vs Ag/AgCl for anodic and cathodic conditions, respectively (Figure 1h). The OCP vs Ag/AgCl was measured as −0.16 V in the $CaSO_4$ and −0.21 V in the silicate feed streams. The OCP of an oil−water emulsion using a CNT-coated membrane and Pt-coated Ti as the electrode pair was −0.13 V in a 0.1 M NaCl solution.[39] The OCP observed in our system is slightly higher for $CaSO_4$ (−0.16 V) and significantly higher for silicate (−0.21 V). Another study comparing the OCP of DI water to a 0.15 M KCl solution showed that solutions with higher ionic strength typically have lower OCPs (0.3 V for 0.15 M KCl and 0.38 V


https://dx.doi.org/10.1021/acs.est.9b07806
Environ. Sci. Technol. XXXX, XXX, XXX−XXX

for DI water, respectively).[40] The $CaSO_4$ solution, with an ionic strength of 0.139 M, had a lower OCP (−0.16 V), while the silicate solution, with an ionic strength of 0.037 M, had a higher OCP (−0.21 V), in agreement with previous reports.[41] The current response measurements showed that under 2 $V_{DC}$ conditions, the steady-state current decreased to 354 ± 17 and 313 ± 9 μA from initial values of 873 ± 30 and 814 ± 51 μA (for $CaSO_4$ and silicate, respectively). This resulted in a current density (normalized to the membrane surface area) of 0.09 A $m^{-2}$. Under 2 $V_{AC,1Hz}$ conditions (Figure S3), the peak current was identical in each cycle during charging and discharging phases, after reaching the steady state, for both feed solutions (880 μA for $CaSO_4$ and 810 μA for silicate). The salt rejection achieved by the membrane exceeded 99% in all experiments.

**3.2. Membrane Distillation Performance.** During all experiments, the initial water flux (time zero) through all membranes ranged between 38 and 43 LMH when the salt solution was used as the feed. These values were similar to the pure water flux measured through the uncoated PP membrane (39.2 LMH), but were lower than the pure water flux through the CNT/PVA membrane composite (51.7 LMH). The presence of the solute in the feed alters the vapor pressure, density, and viscosity and also affects heat transfer due to a change in heat capacity and thermal conductivity. Typically, salts present in feed water lower the flux.[42] It is not clear why the presence of salt lowered flux through the CNT/PVA membrane but did not impact the flux through the uncoated PP membrane.

Scaling occurs when ions accumulate in the CP layer with the highest concentrations at the membrane surface and decaying from there out into the bulk.[43] Supersaturation conditions are likely to develop in the CP layer first, leading to heterogeneous crystal nucleation and growth on the membrane surface, resulting in flux decline.[44] Because our experiments were operated using constant feed conditions (i.e., not in concentration mode), the ion concentrations along the membrane surface (i.e., inside the CP layer) could be calculated using eqs S1−S14. Based on these equations and visual MINTEQ, the SI values along the membrane surface were determined to be 2.28 and 3.18 for $CaSO_4$ and silicate, respectively. These values indicate that supersaturated conditions did indeed develop along the membrane surface, and mineral scaling would likely occur given sufficient time. Importantly, an SI of 2.3 is considered the highest SI where antiscalant chemicals are capable of minimizing $CaSO_4$ scaling, emphasizing the difficult nature of the operating conditions employed herein.[45] We estimated membrane surface temperature (using eqs S1−S14) to be 70 °C on the feed side and 27 °C on the permeate side (with bulk temperatures of 78 and 20 °C, respectively), resulting in a temperature polarization coefficient of 0.74. While electrothermal heating of the membrane is possible, the required electrical power needed to significantly raise the surface temperature is far higher than what was applied here (0.0008 W). Therefore, it is unlikely that the application of the surface potentials in this study would lead to any significant surface temperature increase.

The normalized (to time zero) flux during the treatment of solutions prone to $CaSO_4$ and silicate scaling can be seen in Figure 2a,b, respectively; the average flux decline rate (LMH $h^{-1}$), determined by fitting a linear function through the data points, can be seen in Figure 2c,d, along with the associated $R^2$ values. Figure 2c,d also shows induction time for flux decline under different applied potentials. Based on the SI calculated for the two feed solutions, we anticipated that the time scales for scaling would be significantly different. As expected, the silicate solution, having a higher SI, scaled the membrane in a much shorter time span. In addition to the high SI of the silicate solution, previous studies have demonstrated that the presence of certain cations, such as calcium and magnesium, promote silicate nucleation and polymerization during the fouling of MD membranes.[46]

During the scaling experiments, some of the runs exhibited two distinct flux regimes: an initial period of no flux decline (i.e., the induction period) and a period where flux decline occurred (Figure 2). However, these two regimes were not obvious in all experiments. For example, during the experiments with the uncoated membrane, rapid flux decline was immediately observed (Figure 2a,b). We fitted linear functions through the region where flux decline did occur for each experimental condition tested (Figure 2a,b). Nghiem and Cath (2011) reported that the induction period of $CaSO_4$ and silicate scaling manifested as a period with no flux decline, followed by a period of rapid flux decline and scaling. Similar observations were made during the scaling of NaCl.[47] In our most successful experimental runs, there was a long induction time, with only slow flux decline observed later on during the experiments (e.g., when 2 $V_{AC,1Hz}$ were applied, Figure 2a,b).

Because the trends in flux decline as a function of the applied surface potential were similar, we will discuss the results of $CaSO_4$ and silicate scaling together. In both cases, the uncoated PP membrane exhibited rapid flux decline, with flux decline rates of 10 and 25 LMH $h^{-1}$, respectively (Figure 2c,d). These rates are in-line with the higher SI of the silicate solution, which would lead to more rapid precipitation relative to $CaSO_4$. The higher SI increases the probability of reaching supersaturation conditions in the CP layer. This rapid flux decline is also in agreement with prior studies where flux decline for silicate solutions begins instantly while scaling by $CaSO_4$ has a non-zero induction period.[48] Several striking observations emerge when viewing the scaling results on the CNT/PVA membranes. Simply coating the PP support with the CNT/PVA composite increased the induction period for $CaSO_4$ from 40 to 60 min and lowered the rate of both $CaSO_4$ and silicate scaling, reducing the rate of flux decline from 10 to 3.75 LMH $h^{-1}$ for $CaSO_4$ (a 62.5% decline) and from 25 to 18 LMH $h^{-1}$ for silicate (a 28% decline) (Figure 2c,d). This is in-line with previous reports that indicate that the addition of a hydrophilic layer (i.e., CNT/PVA) onto the hydrophobic MD membrane reduces the degree of scaling. In general, hydrophilic surfaces are more resistant to scaling due to the presence of a tightly bound water layer at the membrane/water interface, which minimizes the attachment of foulants, including mineral scale.[49] The surface roughness of the CNT/PVA-coated membrane is less than that of the bare PP support (390 ± 68 vs 121 ± 20 nm). This could also be a contributing factor to the reduced flux decline rate in the tests with the CNT/PVA-coated membrane, since surface roughness has been shown to impact mineral scaling, with more rough surfaces being more prone to scaling.[50]

For the case of $CaSO_4$ scaling, the application of a 2 $V_{DC}$ cell potential did not increase the induction time, but did result in a drop in the rate of flux decline (compared to the 0 V), from 3.75 to 1.35 LMH $h^{-1}$ (a 64% decline). For the silicate system, 2 $V_{DC}$ cell potential increased the induction time to 40 min and reduced the rate of flux decline from 18 to 12.5 LMH $h^{-1}$ (a


https://dx.doi.org/10.1021/acs.est.9b07806
Environ. Sci. Technol. XXXX, XXX, XXX−XXX

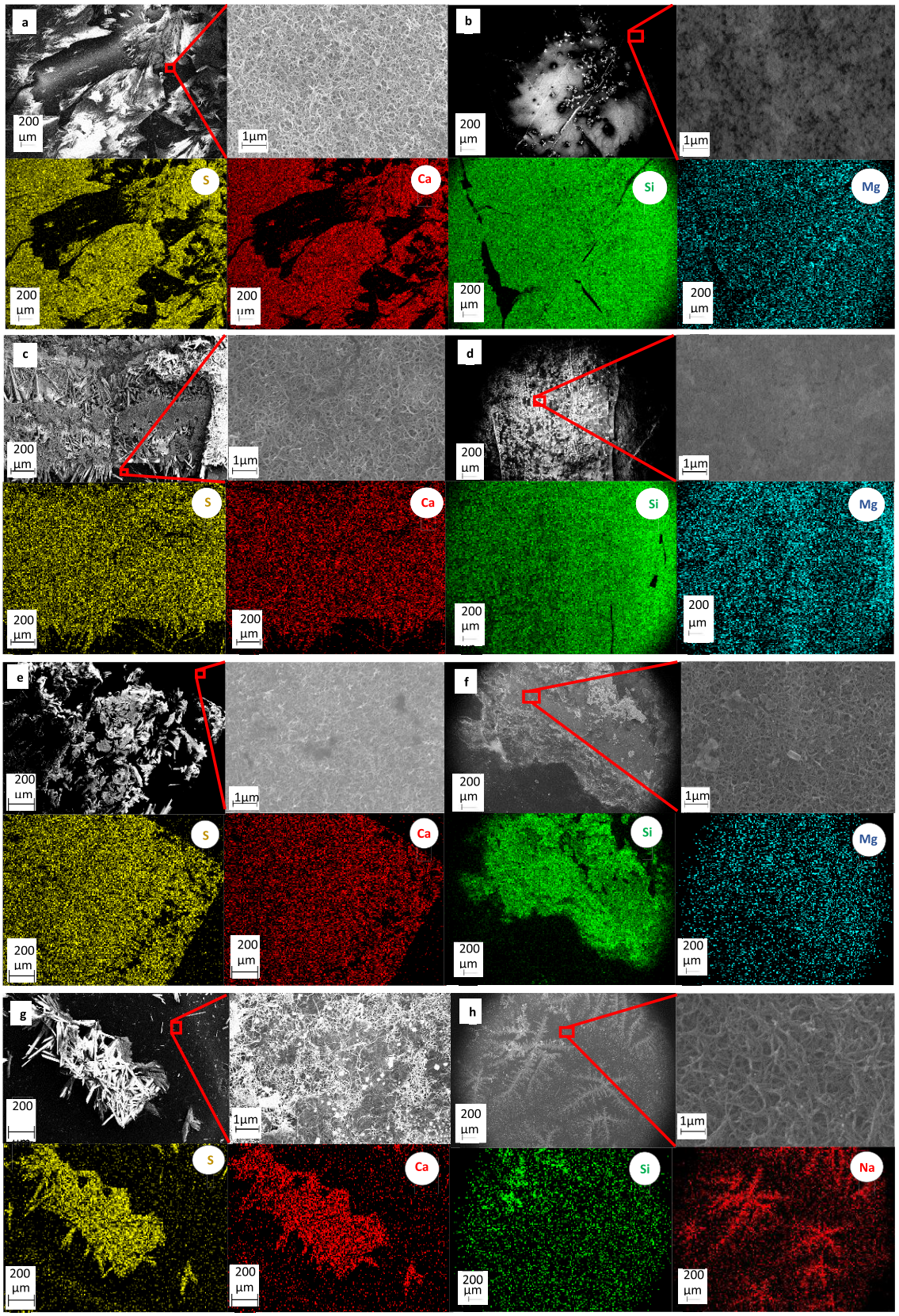


**Figure 3.** SEM and EDAX micrographs of the membrane surface post-scaling experiments under different applied electrical conditions (a) $CaSO_4$, 0 V; (b) silicate, 0 V; (c) $CaSO_4$, 2 $V_{DC}$; (d) silicate, 2 $V_{DC}$; (e) $CaSO_4$, 2 $V_{AC,10Hz}$; (f) silicate, 2 $V_{AC,10Hz}$; (g) $CaSO_4$, 2 $V_{AC,1Hz}$; and (h) silicate 2 $V_{AC,1Hz}$.

30% decline) (Figure 2a−d). There is a possibility that the enhanced performance due to the applied potential may have been caused by a change in pH at the membrane surface. Under 2 $V_{DC}$ potential, we used eq S15 to estimate the pH at


https://dx.doi.org/10.1021/acs.est.9b07806
Environ. Sci. Technol. XXXX, XXX, XXX−XXX

the surface and obtained a surface pH of 10 for silicate and 6.9 for calcium sulfate. This represents a negligible change in surface pH conditions. When AC conditions were used, the net change in pH is likely zero. Therefore, changing pH conditions are not likely to contribute to the observed phenomena. When an AC potential was applied to the membrane, the results were significantly different than the DC conditions. During $CaSO_4$ scaling, when 2 $V_{AC,10Hz}$ were applied, the flux decline was faster than the 2 $V_{DC}$ case (with a rate of 2.82 vs 1.35 LMH $h^{-1}$), and no induction period was apparent (Figure 2a,c). However, when the silicate solution was treated during the application of 2 $V_{AC,10Hz}$, the flux decline rate decreased to 8 LMH $h^{-1}$, down from 12.5 LMH $h^{-1}$ under 2 $V_{DC}$. It is unclear why the silicate solution exhibited better performance under these conditions (2 $V_{AC,10Hz}$), while the $CaSO_4$ performed worse.

For both scaling solutions, the best performance was observed when 2 $V_{AC,1Hz}$ cell potential was applied to the membrane surface. For the $CaSO_4$ case, the induction period increased dramatically to 200 min, and the flux decline rate declined to 0.7 LMH $h^{-1}$ (81% smaller than at 0 V). For silicate, the induction time increased to 100 min, and the rate of flux decline decreased to 3.8 LMH $h^{-1}$ (79% decrease vs 0 V). However, when the pH of the silicate-rich feed solution was decreased to 6, the rate of flux decline increased to 4.2 LMH $h^{-1}$ (when 2 $V_{AC,1Hz}$ were applied) and the induction period decreased to 20 min (Figure 2b). At lower pH conditions, silicate solutions are less soluble, which could cause silicates to precipitate at pH 6, resulting in increased flux decline. To evaluate this possibility, we conducted a control experiment with the CNT-coated membrane and no potential applied (0 V) and a silicate solution at a pH of 6 (Figure 2b). Under these conditions, the flux decline rate was 18.44 LMH $h^{-1}$ (Figure 2d). This was very similar to the flux decline rate under 0 V at pH 10 (18.08 LMH $h^{-1}$). Based on this, the increased membrane scaling observed under the lower pH conditions (at 2 $V_{AC,1Hz}$ conditions) cannot be attributed to enhanced precipitation of silicate in the solution. Hence, we can rule out bulk precipitation as the cause for the increased flux decline rate under 2 $V_{AC,1Hz}$ conditions for the silicate solution at pH 6.

Since the exact speciation of the silicates in our feed solutions is impossible to predict (and is likely a mix of several species), it is likely that reducing the pH of the feed solution will transform some (or all) of the silicates to their noncharged forms, which will not respond (or respond to a lesser extent) to the applied electrical potential.[51] Thus, it is not surprising that the membrane flux started declining after a shorter time and the rate of flux decline was faster, as silicate scaling was not effectively prevented through the application of potential. Since $CaSO_4$ is insensitive to pH changes, we do not expect the scaling behavior of the $CaSO_4$ solution to change at a reduced pH. From the above results and from Figure 2c,d, it is evident that the membrane surface properties, applied electric potential, and solution pH (in the case of silicate) had a significant impact on the rate of flux decline and induction time.

**3.3. Membrane Surface Characterization after Scaling.** We have provided pictures of the scaled membrane surface for visual inspection of the scaling layer (Figure S4). A dense scaling layer is observed under 0 V conditions for both feed solutions. In the test with $CaSO_4$, the rate of flux decline was faster under conditions of 2 $V_{AC,10Hz}$ than 2 $V_{DC}$ (2.82 vs 1.35 LMH $h^{-1}$), and we expected to see a more densely scaled layer on the membrane scaled under 2 $V_{AC,10Hz}$ conditions. However, the surface of the membrane scaled under 2 $V_{DC}$ conditions appeared to be more densely coated with the $CaSO_4$ scale. The reason for this is not clear. They were both less densely coated than the membrane scaled under 0 V conditions. For the silicate-scaled membrane, the surface coverage appeared to be similar for 2 $V_{DC}$ and 2 $V_{AC,10Hz}$ (both less dense than 0 V conditions). The surface of the membrane scaled under conditions of 2 $V_{AC,1Hz}$ was sparsely covered by a scaling layer for membranes scaled by both solutions. This agrees with our experimental results that 2 $V_{AC,1Hz}$ conditions provide the best scaling resistance. SEM images were used to qualitatively assess membrane scaling. A SEM micrograph of a $CaSO_4$-scaled CNT/PVA-coated membrane with no potential revealed a mixture of needle-like and plate-like crystals (Figure 3a). Past investigations have shown that the morphology of crystals depends on the SI and crystallization kinetics.[16,52] Needle-like crystallization is observed when crystals formed in the bulk phase (due to formation of nuclei in the bulk phase and subsequent attachment on dissolved ions) attach to the membrane surface (bulk crystallization), while plate-like formations are observed when crystal growth occurs on the membrane surface (due to the formation of nuclei on the membrane surface and subsequent deposition of dissolved ions) (surface crystallization).[53] EDAX analysis showed that the membrane was primarily covered by a thick layer of calcium and sulfur (Figure 3a). XRD analysis of the membrane scaled under 0 V (Figure S5a) showed a diffractogram that can be associated with the presence of gypsum, with peaks at $2\theta$ values of 11.6, 20.5, 23.4, and 29.07.[54]

On the silicate-scaled membrane, a uniform colloidal layer was observed covering the surface (Figure 3b). This is consistent with past studies that show the polymerization of silicate monomers in the presence of divalent cations results in a colloidal, gel-like scaling layer.[55] Some structures were observed deposited on top of this silicate scaling layer. EDAX analysis of the deposits indicated that the surface was covered by silicon- and magnesium-containing minerals (Figure 3b). XRD analysis of the silicate-scaled membrane (Figure S5b) did not reveal diffraction patterns that could be associated with any major silica-containing crystals. This is likely due to the amorphous gel-like layer of silicates on the fouled membrane surface.

A SEM micrograph of the CNT/PVA membrane surface after 2 $V_{DC}$ cell potential was applied while treating the $CaSO_4$ solution shows a large number of needle-like crystals that are characteristic of bulk crystallization,[29,56] suggesting that bulk crystallization dominates scaling under 2 $V_{DC}$ conditions (Figure 3c). SEM and EDAX analyses of the silicate-scaled membrane after the application of 2 $V_{DC}$ showed a similar colloidal layer interspersed with a larger number of plate-like structures (Figure 3d), indicating more scaling on the surface. SEM micrographs of the membrane surface after the application of 2 $V_{AC,10Hz}$ showed uniform crystal deposition throughout the membrane surface for both the $CaSO_4$ and silicate-scaled membranes (Figure 3e). SEM micrographs of the $CasO_4$-scaled membrane after 2 $V_{AC,1Hz}$ were applied to the membrane surface revealed a very sparse cover of sharp needle-like crystals, similar to those formed by the crystallization of gypsum in bulk liquid.[16] A zoomed-in micrograph revealed the presence of smaller crystals (150 nm) on the surface (Figure 3g). In Figure 3h, the silicate-scaled membrane was not as


https://dx.doi.org/10.1021/acs.est.9b07806
Environ. Sci. Technol. XXXX, XXX, XXX−XXX

thoroughly covered by silicon. For both $CaSO_4$ and silicate-scaled membranes, the CNT network was visible in the SEM micrographs, indicating poor surface coverage when 2 $V_{AC,1Hz}$ were applied. These observations match our flux decline observations, where under the 2 $V_{AC,1Hz}$ conditions, the membrane experienced dramatically less flux decline.

**3.4. Proposed Mechanism of Scaling Inhibition.** Mineral scaling is induced by supersaturated conditions, which in our system can rapidly develop due to concentration polarization adjacent to the membrane (Figure 4a). It has been shown, using $CaCO_3$, that nanoscale amorphous prenucleation clusters rapidly form on the time scale of seconds in areas where supersaturation conditions exist in the bulk liquid phase. These clusters then attach to a surface and serve as a template for further (and rapid) crystal growth due to the deposition of ions from the solution.[25,57] A similar phenomenon has been observed with hemihydrate $CaSO_4$.[58] In our previous work, we observed that the application of a 1.5 $V_{DC}$ cell potential to the surface of an electrically conducting RO membrane slowed the rate of $CaSO_4$ scaling.[10] The mechanism responsible for the observed antiscaling phenomena was hypothesized to be the formation of a thick EDL along the membrane surface. When a DC potential is applied, counter ions from the bulk solution are attracted to the membrane surface (forming the EDL structure within the CP layer), which creates an imbalance in the concentration of anions and cations (Figure 4b). It has been demonstrated that the rate of nucleation is impacted by the degree of saturation and by the availability of both anions and cations to come together and form the crystal structure, with the highest rates occurring when the ratio between anions and cations is stoichiometric.[59,60] Thus, in the EDL, where there is an imbalance between anion and cation concentrations (pushing the ratio away from stoichiometry), the nucleation rate is lower. The EDL thickness was calculated using the Debye−Huckel theory (eq S16) and found to be 1.46 nm for calcium sulfate scaling solution and 2.64 nm for silicate scaling solution, while the CP layer can vary in thickness from a few microns to a few hundred microns.[61] Therefore, this imbalance does not extend throughout the CP layer, and as a result, the nucleation zone is only pushed a short distance away from the membrane surface (Figure 4b).[27,62] Thus, just a few nm away from the membrane surface (i.e., outside of the EDL), the ratio between anions and cations returns to that which enables rapid scale formation and prenucleation clusters can be formed under these conditions. That being said, the newly formed prenucleation clusters have to transport over a longer distance to reach the membrane surface, and once there, the imbalance between the anions and cations slows further crystal growth. When considering membrane roughness and the thinness of the EDL relative to the CP layer, it becomes clear that a DC potential, while capable of slowing down nucleation, cannot completely prevent scaling, which is evident by our experimental results presented in Figure 2. Furthermore, since applying DC potential pushes the nucleation zone away from the membrane surface, bulk crystallization is expected to dominate the scaling process. Our SEM micrographs of the 2 $V_{DC}$ condition (Figure 3c,d) show needle-like deposits, which are characteristic of bulk crystallization.

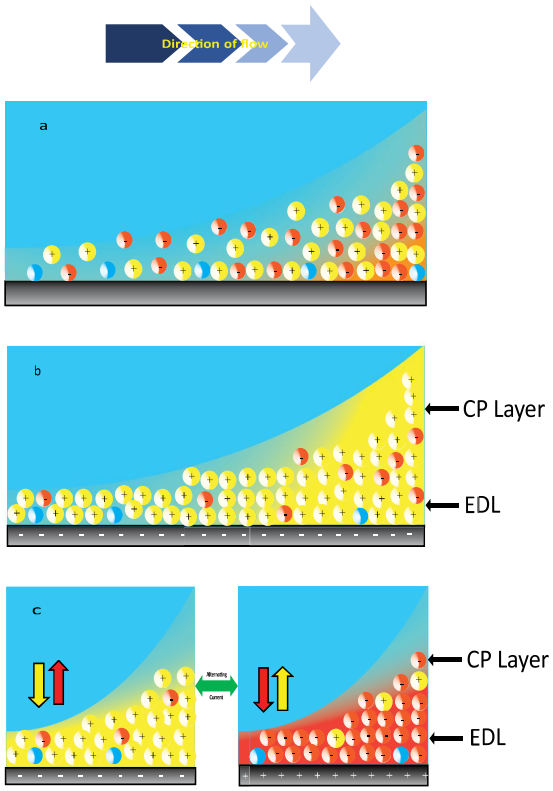


**Figure 4.** Graphical representation of scaling mitigation by electrophoretic mixing. (a) Formation of the CP layer near the surface of an uncharged membrane; (b) formation of EDL near the membrane surface through the application of 2 $V_{DC}$ potential (membrane as the cathode); (c) electrophoretic mixing within the CP layer due to EDL disruption and reformation caused by switching the polarity of the membrane.

In contrast to the steady EDL formed in response to a DC potential, the application of an AC potential periodically forms and disrupts the EDL, with the periodicity of this disruption dependent on the frequency of the applied electrical potential.[63] When the field direction is changed, anions and cations move in opposite directions in response to the field, potentially leading to electrophoretic "mixing" within the CP layer (Figure 4c). Studies on the current response during the charging and discharging of the EDL show that the current is highest at the instance when a potential is applied and exponentially decreases as the EDL is formed, reaching a constant value after complete formation of the EDL. Thus, if the polarity of the electrode is switched at a sufficiently rapid rate, this ion flux (current) can be maintained at a higher rate to encourage better mixing. In our current response curves (Figure S3), for calcium sulfate, the initial peak current of 880 $\mu$A decreases to 480 $\mu$A before changing direction (when the polarity is changed) and immediately surging to 880 $\mu$A in the opposite direction. For silicate (Figure S3b), the initial peak current is 810 $\mu$A, which decreases to 390 $\mu$A before changing direction and immediately surging to 810 $\mu$A (when the polarity is switched). Thus, switching polarity at a rapid rate will induce movement of ions, encourage mixing, and prevent the formation of prenucleation clusters by preventing co-location of scale-forming ions. We hypothesize that this mixing may extend beyond the boundaries of the EDL, thus promoting longer-range disruption of ion concentrations along the membrane surface. This disruption limits the time anions and cations spend in close proximity in the near-membrane region, which limits the formation of prenucleation clusters critical for heterogeneous nucleation.[64] Importantly, it is unlikely that the ion migration will result in significant water


https://dx.doi.org/10.1021/acs.est.9b07806
Environ. Sci. Technol. XXXX, XXX, XXX−XXX

movement, as the applied fields (500 V $m^{-1}$) are relatively weak.[65] We hypothesize that the periodic switching of the membrane's polarity will induce long-distance (i.e., beyond the EDL boundaries) disruption of ion concentrations within the CP layer and that this mixing is due only to the movement of ions and does not result in any bulk liquid motion.

When we reduced the pH of the silicate solution to 6, which transformed silicate monomers primarily to their uncharged state, scaling prevention was curtailed. This strengthens our hypothesis that ion migration in response to the changing electric field is responsible for the observed antiscaling phenomenon.

We explored the role of electrosorption in the CNT network by measuring the specific capacitance of the membranes, which was determined to be 0.54 F $g^{-1}$ (eq S17). This value is significantly lower than the values associated with capacitive deionization CDI electrodes composed of activated carbon (143 F $g^{-1}$).[66] In addition, CV curves typically observed during CDI are rectangular in shape, indicating consistent ionic loading during the charging step, while the CV curves associated with our membranes show limited charging behavior, indicating a limited role of electrosorption in our system (Figure 1g,h).[67,68]

To assess the dynamics of the EDL under a periodically applied potential, we consider the time scale required for "charging" an EDL, the so-called "RC" time scale, $t_{RC} \sim \lambda_D L/D$, in which $\lambda_D$ is the Debye length, characterizing the distance over which the EDL is formed, $L$ is the distance between the electrodes, and $D$ is the diffusivity of the ionic species.[69] Comparing this time scale with that of the applied oscillations, the inverse of the frequency produces a dimensionless parameter $-\tau = \omega\lambda_D L/D$. When $\tau > 1$, phase lags are observed between different regions of the EDL as it responds to the oscillating force.[70] Furthermore, it has been recently shown that if there is a diffusivity mismatch between ionic species, the symmetry breaks down and a long-range, time-averaged electric field is established.[71]

Under the conditions prevailing in our experiments, $\tau \ll 1$, meaning that the EDL is quasi-static and responds instantaneously to the change in potential. In this case, the disruption to the scale formation process is unlikely to be caused by a reduction of the concentrations below supersaturation. Rather, we hypothesize that the shift in local ionic composition during the polarity switch reduces the co-location of anions and cations to a time scale small enough to minimize the formation of the prenucleation clusters. These ideas are motivated by our experimental data that show a dramatic decline in scaling when an AC potential is applied to the membrane, as well as SEM micrographs that show far less crystal formation on the membrane surface under AC conditions. This is further supported by experimental evidence showing that prenucleation clusters form over a time scale in the order of seconds under supersaturated conditions, hence, when the electrophoretic motion is sufficiently frequent (i.e., the membrane polarity is switched at a high enough frequency), anions and cations will not be co-located for the amount of time necessary to induce the formation of these prenucleation clusters.

Based on this hypothesized mechanism and the diffusivity mismatch present in our system, it would seem that higher frequencies would lead to better performance (moving away from the quasi-static regime). Higher frequency would cause a more rapid mixing of ions and should be more effective at preventing co-location of scale-forming ions. However, in our experiments, we clearly observed increased fouling when operating at 10 vs 1 Hz (Figures 2 and 3). In an attempt to understand this discrepancy, we conducted EIS measurements to determine the capacitive behavior of the conducting membranes under different applied frequencies (Figure S6). In Figure S6, the phase shift vs the applied frequency (i.e., a Bode plot) is displayed for the ECMD and a Pt-coated Ti sheet as working electrodes in both the $CaSO_4$ and silicate feed solutions. In EIS measurements, a negative phase shift indicates the capacitive charging of the EDL.[72] When no phase shift is measured, this typically means the system is acting more like a resistor. When the ECMD membrane was used as the working electrode in the $CaSO_4$ solution, the phase shifts were −2.8 and −3.6° at 10 and 100 Hz, respectively; in the silicate solution, the phase shifts were −1.6 and −1.2° at 10 and 100 Hz, respectively. These values are very low and indicate that at these frequencies, little capacitive charging is taking place, and the ECMD material is functioning primarily as a resistor, with little EDL formation. However, at 1 Hz, the phase shift was measured to be −14.7 and −14.2° for the $CaSO_4$ and silicate solutions, respectively. These larger phase shift values indicate that the material is indeed acting more like a capacitor with an EDL associated with it. This could possibly be due to the relatively high electrical resistance of the ECMD (228 ± 14 Ω/square), which was preventing effective charge distribution across the membrane surface, which prevented the formation of a robust EDL when high frequencies were applied. To test this hypothesis, we performed identical EIS measurements using a Pt-coated Ti sheet as a working electrode (Figure S6); the Pt-coated Ti had a very low sheet resistance ($8 \times 10^{-4} \pm 9.6 \times 10^{-5}$ Ω/square), and thus, we anticipated that this material would express capacitive charging at higher frequencies. Indeed, when the highly conducting material was used, a large phase shift (−31.7°) was observed at 10 Hz (in the $CaSO_4$ solution), with a larger shift (−57.4°) at 1 Hz. A similar behavior was observed in the silicate solution. While not a perfect comparison (the solid metal sheet is not identical to a porous CNT electrode, which can impact the way ions interact with the surface and would require different circuit elements when constructing equivalent circuits to describe these systems), this comparison is meant to illustrate the impact of conductivity on capacitive charging. Therefore, we conclude that the poor antiscaling performance observed at 10 Hz using the ECMD material is a result of the material's inability to effectively distribute charge throughout its surface at this frequency (due to the short period of time before polarity is switched). This ineffective charge distribution will prevent the EDL from fully forming and be unable to influence the ions to move within the CP layer. This results in poor electrophoretic mixing. However, if a membrane material with a lower resistance could be fabricated, we anticipate that higher operating frequencies would yield better antiscaling performance due to the fact that a more conductive membrane material would enable faster charge distribution through the surface, allowing the EDL to fully form before the potential is switched. In our system, due to poor conductivity and charge distribution, there is a reduced driving force for the ions in solution to respond to the applied potential, due to the incomplete formation of the electric field (as a result of inefficient charge distribution).

In summary, an effective antiscaling method was developed, which significantly reduced the occurrence of $CaSO_4$ and


https://dx.doi.org/10.1021/acs.est.9b07806
Environ. Sci. Technol. XXXX, XXX, XXX−XXX

silicate scaling on ECMD membrane surfaces. When an electrical potential was applied to the membrane surface, the occurrence of mineral scaling could be greatly reduced, with the frequency of the applied potential having a dramatic impact on the scaling rate. In our experiments, AC conditions performed better than DC conditions due to the mixing within the EDL. We hypothesize that this reduces the opportunity for anions and cations to co-exist in the same space under supersaturated conditions and prevents them from forming prenucleation clusters needed to form larger crystals. We identified 2 $V_{AC,1Hz}$ as the optimal electrical condition that minimized both $CaSO_4$ and silicate scaling to the largest extent. While we expect that higher frequencies will improve the performance of the system, the relatively poor electrical properties of our conducting membrane limited the capacitive charging behavior to relatively lower frequencies. Improving the membrane's conductivity is expected to allow higher operating frequencies, which should improve antiscaling performance. Over a 5 year period, power requirements are 180 kWh $m^{-2}$ for this treatment process. An economic analysis (details in the Supporting Information) indicated that the additional costs associated with the optimal antiscaling performance are \$0.024 per $m^3$ of water produced. In terms of savings, these costs need to be compared to the cost of antiscalants and brine disposal, which vary depending on the physical location and the chemical composition of the water requiring treatment.

## ■ ASSOCIATED CONTENT

### Supporting Information

The Supporting Information is available free of charge at https://pubs.acs.org/doi/10.1021/acs.est.9b07806.

> Composition of the calcium sulfate and silicate feed solutions (Tables S1 and S2); saturation indices of minerals that could potentially precipitate in the feed during the desalination of silicate solution (Figure S1); system process diagram (Figure S2); chronoamperometry curves with the CNT membrane and the metal plate (Pt−Ti) as electrodes for (a) $CaSO_4$ and (b) silicate solution (Figure S3); calculation of saturation indices along the membrane surface (Eqs S1−S14); modeling surface pH under the influence of applied potential (Eq S15); pictures of the (a) $CaSO_4$ and (b) silicate-scaled membranes under different operating conditions (Figure S4); calculating EDL thickness (Eq S16); X-ray diffractogram of the (a) $CaSO_4$ and (b) silicate-scaled membranes (Figure S5); phase shift vs frequency with a highly conductive metal plate (Pt−Ti) as the working electrode (black) and the CNT membrane as the working electrode (red) for (a) $CaSO_4$ and (b) silicate solution (Figure S6); economic analysis (Eq S17) (PDF)

## ■ AUTHOR INFORMATION


### Corresponding Author

**David Jassby** − *Department of Civil and Environmental Engineering, University of California, Los Angeles, California 90095-153, United States;* orcid.org/0000-0002-2133-2536; Email: jassby@ucla.edu

### Authors

**Unnati Rao** − *Department of Civil and Environmental Engineering, University of California, Los Angeles, California 90095-153, United States*

**Arpita Iddya** − *Department of Civil and Environmental Engineering, University of California, Los Angeles, California 90095-153, United States*

**Bongyeon Jung** − *Department of Civil and Environmental Engineering, University of California, Los Angeles, California 90095-153, United States*

**Chia Miang Khor** − *Department of Civil and Environmental Engineering, University of California, Los Angeles, California 90095-153, United States*

**Zachary Hendren** − *RTI International, Research Triangle Park, North Carolina 27709, United States*

**Craig Turchi** − *Department of Energy, National Renewable Energy Lab, Golden, Colorado 80401, United States*

**Tzahi Cath** − *Department of Civil and Environmental Engineering, Colorado School of Mines, Golden, Colorado 80401, United States*

**Eric M. V. Hoek** − *Department of Civil and Environmental Engineering, University of California, Los Angeles, California 90095-153, United States;* orcid.org/0000-0002-5748-6481

**Guy Z. Ramon** − *Department of Civil and Environmental Engineering, Technion-Israel Institute of Technology, Haifa 32000, Israel;* orcid.org/0000-0002-0711-0654

Complete contact information is available at: https://pubs.acs.org/10.1021/acs.est.9b07806


### Notes

The authors declare no competing financial interest.

## ■ ACKNOWLEDGMENTS

This work was undertaken in collaboration with the U.S. Department of Energy's National Renewable Energy Laboratory (NREL) with funding under subcontract AEJ-9-82309-01 and prime contract DE-AC36-08GO28308. In addition, the work was supported by the National Science Foundation CAREER Award (1553756). We would like to thank Steven Bustillos and Gaurav Sant for their help with XRD measurements.

## ■ REFERENCES


(1) Amy, G.; Ghaffour, N.; Li, Z.; Francis, L.; Linares, R. V.; Missimer, T.; Lattemann, S. Membrane-based seawater desalination: Present and future prospects. *Desalination* **2017**, *401*, 16−21.

(2) Tang, L.; Iddya, A.; Zhu, X.; Dudchenko, A. V.; Duan, W.; Turchi, C.; Vanneste, J.; Cath, T. Y.; Jassby, D. Enhanced Flux and Electrochemical Cleaning of Silicate Scaling on Carbon Nanotube-Coated Membrane Distillation Membranes Treating Geothermal Brines. *ACS Appl. Mater. Interfaces* **2017**, *9*, 38594−38605.

(3) Alkhudhiri, A.; Darwish, N.; Hilal, N. Membrane distillation: a comprehensive review. *Desalination* **2012**, *287*, 2−18.

(4) Curcio, E.; Drioli, E. Membrane distillation and related operations—a review. *Sep. Purif. Rev.* **2005**, *34*, 35−86.

(5) Schofield, R.; Fane, A.; Fell, C. Heat and mass transfer in membrane distillation. *J. Membr. Sci.* **1987**, *33*, 299−313.

(6) Khayet, M.; Matsuura, T. *Membrane Distillation: Principles and Applications*; Elsevier, 2011.

(7) Rao, U.; Posmanik, R.; Hatch, L. E.; Tester, J. W.; Walker, S. L.; Barsanti, K. C.; Jassby, D. Coupling hydrothermal liquefaction and membrane distillation to treat anaerobic digestate from food and dairy farm waste. *Bioresour. Technol.* **2018**, *267*, 408−415.

(8) Dudchenko, A. V.; Rolf, J.; Russell, K.; Duan, W.; Jassby, D. Organic fouling inhibition on electrically conducting carbon nanotube−polyvinyl alcohol composite ultrafiltration membranes. *J. Membr. Sci.* **2014**, *468*, 1−10.
(9) Khayet, M. Membranes and theoretical modeling of membrane distillation: a review. *Adv. Colloid Interface Sci.* **2011**, *164*, 56−88.
(10) Duan, W.; Dudchenko, A.; Mende, E.; Flyer, C.; Zhu, X.; Jassby, D. Electrochemical mineral scale prevention and removal on electrically conducting carbon nanotube−polyamide reverse osmosis membranes. *Environ. Sci.: Processes Impacts* **2014**, *16*, 1300−1308.
(11) Elimelech, M.; Bhattacharjee, S. A novel approach for modeling concentration polarization in crossflow membrane filtration based on the equivalence of osmotic pressure model and filtration theory. *J. Membr. Sci.* **1998**, *145*, 223−241.
(12) Kim, S.; Hoek, E. M. Modeling concentration polarization in reverse osmosis processes. *Desalination* **2005**, *186*, 111−128.
(13) Song, L.; Elimelech, M. Theory of concentration polarization in crossflow filtration. *J. Chem. Soc., Faraday Trans.* **1995**, *91*, 3389−3398.
(14) Andritsos, N.; Karabelas, A. Calcium carbonate scaling in a plate heat exchanger in the presence of particles. *Int. J. Heat Mass Transfer* **2003**, *46*, 4613−4627.
(15) Franken, A.; Nolten, J.; Mulder, M.; Bargeman, D.; Smolders, C. Wetting criteria for the applicability of membrane distillation. *J. Membr. Sci.* **1987**, *33*, 315−328.
(16) Antony, A.; Low, J. H.; Gray, S.; Childress, A. E.; Le-Clech, P.; Leslie, G. Scale formation and control in high pressure membrane water treatment systems: a review. *J. Membr. Sci.* **2011**, *383*, 1−16.
(17) Amjad, Z. *Mineral Scale Formation and Inhibition*; Springer Science & Business Media, 2013.
(18) Fu, F.; Wang, Q. Removal of heavy metal ions from wastewaters: a review. *J. Environ. Manage.* **2011**, *92*, 407−418.
(19) Younos, T. Environmental issues of desalination. *J. Contemp. Water Res. Educ.* **2005**, *132*, 11−18.
(20) Sheikholeslami, R.; Watkinson, A. Scaling of plain and externally finned heat exchanger tubes. *J. Heat Transfer* **1986**, *108*, 147−152.
(21) Watkinson, A.; Martinez, O. Scaling of heat exchanger tubes by calcium carbonate. *J. Heat Transfer* **1975**, *97*, 504−508.
(22) Shirazi, S.; Lin, C.-J.; Chen, D. Inorganic fouling of pressure-driven membrane processes—a critical review. *Desalination* **2010**, *250*, 236−248.
(23) Auer, S.; Frenkel, D. Line tension controls wall-induced crystal nucleation in hard-sphere colloids. *Phys. Rev. Lett.* **2003**, *91*, No. 015703.
(24) Mi, B.; Elimelech, M. Gypsum scaling and cleaning in forward osmosis: measurements and mechanisms. *Environ. Sci. Technol.* **2010**, *44*, 2022−2028.
(25) Pouget, E. M.; Bomans, P. H.; Goos, J. A.; Frederik, P. M.; de With, G.; Sommerdijk, N. A J. M. The initial stages of template-controlled CaCO3 formation revealed by cryo-TEM. *Science* **2009**, *323*, 1455−1458.
(26) Gryta, M. Calcium sulphate scaling in membrane distillation process. *Chem. Pap.* **2009**, *63*, 146−151.
(27) Lyster, E.; Kim, M.-m.; Au, J.; Cohen, Y. A method for evaluating antiscalant retardation of crystal nucleation and growth on RO membranes. *J. Membr. Sci.* **2010**, *364*, 122−131.
(28) Rahardianto, A.; McCool, B. C.; Cohen, Y. Reverse osmosis desalting of inland brackish water of high gypsum scaling propensity: kinetics and mitigation of membrane mineral scaling. *Environ. Sci. Technol.* **2008**, *42*, 4292−4297.
(29) Shih, W.-Y.; Rahardianto, A.; Lee, R.-W.; Cohen, Y. Morphometric characterization of calcium sulfate dihydrate (gypsum) scale on reverse osmosis membranes. *J. Membr. Sci.* **2005**, *252*, 253−263.
(30) Hasson, D.; Drak, A.; Semiat, R. Inception of CaSO4 scaling on RO membranes at various water recovery levels. *Desalination* **2001**, *139*, 73−81.
(31) Nghiem, L. D.; Cath, T. A scaling mitigation approach during direct contact membrane distillation. *Sep. Purif. Technol.* **2011**, *80*, 315−322.
(32) Ahmed, F.; Lalia, B. S.; Kochkodan, V.; Hilal, N.; Hashaikeh, R. Electrically conductive polymeric membranes for fouling prevention and detection: A review. *Desalination* **2016**, *391*, 1−15.
(33) Celik, E.; Park, H.; Choi, H.; Choi, H. Carbon nanotube blended polyethersulfone membranes for fouling control in water treatment. *Water Res.* **2011**, *45*, 274−282.
(34) Duan, W.; Chen, G.; Chen, C.; Sanghvi, R.; Iddya, A.; Walker, S.; Liu, H.; Ronen, A.; Jassby, D. Electrochemical removal of hexavalent chromium using electrically conducting carbon nanotube/polymer composite ultrafiltration membranes. *J. Membr. Sci.* **2017**, *531*, 160−171.
(35) Gustafsson, J. P. Visual MINTEQ. 3.0 User Guide. *KTH, Department of Land and Water Recources*; Stockholm, Sweden, 2011.
(36) Dudchenko, A. V.; Chen, C.; Cardenas, A.; Rolf, J.; Jassby, D. Frequency-dependent stability of CNT Joule heaters in ionizable media and desalination processes. *Nat. Nanotechnol.* **2017**, *12*, 557.
(37) Vaisman, L.; Wagner, H. D.; Marom, G. The role of surfactants in dispersion of carbon nanotubes. *Adv. Colloid Interface Sci.* **2006**, *128−130*, 37−46.
(38) Slade, A.; Jassby, D. Affordable, flexible, and modular: a guide to open-source membrane-based water treatment systems. *Environ. Sci.: Water Res. Technol.* **2016**, *2*, 965−974.
(39) Zhu, X.; Dudchenko, A. V.; Khor, C. M.; He, X.; Ramon, G. Z.; Jassby, D. Field-Induced Redistribution of Surfactants at the Oil/Water Interface Reduces Membrane Fouling on Electrically Conducting Carbon Nanotube UF Membranes. *Environ. Sci. Technol.* **2018**, *52*, 11591−11600.
(40) Stojiljković, A. S.; Sužnjević, D. Ž.; Blagojević, S. N. Open-circuit potential of a Pt electrode immersed in different aqueous solutions. *React. Kinet., Mech. Catal.* **2018**, *123*, 165−175.
(41) Reid, M. A.; Gahn, R. F. FactorsAffecting the Open-Circuit Voltage and Electrode Kinetics of Some Iron/TitaniumRedox Flow Cells, 1977.
(42) Schofield, R.; Fane, A.; Fell, C.; Macoun, R. Factors affecting flux in membrane distillation. *Desalination* **1990**, *77*, 279−294.
(43) Sablani, S.; Goosen, M.; Al-Belushi, R.; Wilf, M. Concentration polarization in ultrafiltration and reverse osmosis: a critical review. *Desalination* **2001**, *141*, 269−289.
(44) Sirkar, K. K.; Rao, G. H. Approximate design equations and alternate design methodologies for tubular reverse osmosis desalination. *Ind. Eng. Chem. Process Des. Dev.* **1981**, *20*, 116−127.
(45) Zhu, A.; Rahardianto, A.; Christofides, P. D.; Cohen, Y. Reverse osmosis desalination with high permeability membranes—cost optimization and research needs. *Desalin. Water Treat.* **2010**, *15*, 256−266.
(46) Niibori, Y.; Kunita, M.; Tochiyama, O.; Chida, T. Dissolution rates of amorphous silica in highly alkaline solution. *J. Nucl. Sci. Technol.* **2000**, *37*, 349−357.
(47) Meng, S.; Mansouri, J.; Ye, Y.; Chen, V. Effect of templating agents on the properties and membrane distillation performance of TiO2-coated PVDF membranes. *J. Membr. Sci.* **2014**, *450*, 48−59.
(48) Bremere, I.; Kennedy, M.; Mhyio, S.; Jaljuli, A.; Witkamp, G.-J.; Schippers, J. Prevention of silica scale in membrane systems: removal of monomer and polymer silica. *Desalination* **2000**, *132*, 89−100.
(49) Ong, C.; Goh, P.; Lau, W.; Misdan, N.; Ismail, A. Nanomaterials for biofouling and scaling mitigation of thin film composite membrane: A review. *Desalination* **2016**, *393*, 2−15.
(50) Vrijenhoek, E. M.; Hong, S.; Elimelech, M. Influence of membrane surface properties on initial rate of colloidal fouling of reverse osmosis and nanofiltration membranes. *J. Membr. Sci.* **2001**, *188*, 115−128.
(51) Provis, J. L.; Duxson, P.; Lukey, G. C.; Separovic, F.; Kriven, W. M.; Van Deventer, J. S. Modeling speciation in highly concentrated alkaline silicate solutions. *Ind. Eng. Chem. Res.* **2005**, *44*, 8899−8908.


https://dx.doi.org/10.1021/acs.est.9b07806
Environ. Sci. Technol. XXXX, XXX, XXX−XXX

(52) Gilron, J.; Hasson, D. Calcium sulphate fouling of reverse osmosis membranes: flux decline mechanism. *Chem. Eng. Sci.* **1987**, *42*, 2351−2360.
(53) Lewis, A.; Nathoo, J.; Seewoo, S.; Lacour, S. In *Prevention of Scaling in Mine Waters Using Slurry Precipitation and Recycle Reverse Osmosis (SPARRO)*, International Symposium on Industrial Crystallization, 2002.
(54) Lafuente, B.; Downs, R. T.; Yang, H.; Stone, N. The Power of Databases: the RRUFF Project. *Highlights in Mineralogical Crystallography*; Walter de Gruyter GmbH, 2016; pp 1−29.
(55) Sheikholeslami, R.; Al-Mutaz, I.; Tan, S.; Tan, S. Some aspects of silica polymerization and fouling and its pretreatment by sodium aluminate, lime and soda ash. *Desalination* **2002**, *150*, 85−92.
(56) Seewoo, S.; Van Hille, R.; Lewis, A. Aspects of gypsum precipitation in scaling waters. *Hydrometallurgy* **2004**, *75*, 135−146.
(57) Gebauer, D.; Völkel, A.; Cölfen, H. Stable prenucleation calcium carbonate clusters. *Science* **2008**, *322*, 1819−1822.
(58) Saha, A.; Lee, J.; Pancera, S. M.; Bräeu, M. F.; Kempter, A.; Tripathi, A.; Bose, A. New Insights into the transformation of calcium sulfate hemihydrate to gypsum using time-resolved cryogenic transmission electron microscopy. *Langmuir* **2012**, *28*, 11182−11187.
(59) Ahmi, F.; Gadri, A. Kinetics and morphology of formed gypsum. *Desalination* **2004**, *166*, 427−434.
(60) Lochhead, M. J.; Letellier, S. R.; Vogel, V. Assessing the role of interfacial electrostatics in oriented mineral nucleation at charged organic monolayers. *J. Phys. Chem. B* **1997**, *101*, 10821−10827.
(61) Pope, J.; Yao, S.; Fane, A. Quantitative measurements of the concentration polarisation layer thickness in membrane filtration of oil-water emulsions using NMR micro-imaging. *J. Membr. Sci.* **1996**, *118*, 247−257.
(62) Pomerantz, N.; Ladizhansky, Y.; Korin, E.; Waisman, M.; Daltrophe, N.; Gilron, J. Prevention of scaling of reverse osmosis membranes by "zeroing" the elapsed nucleation time. Part I. Calcium sulfate. *Ind. Eng. Chem. Res.* **2006**, *45*, 2008−2016.
(63) Talapatra, S.; Chakraborty, S. Double layer overlap in ac electroosmosis. *Eur. J. Mech. B* **2008**, *27*, 297−308.
(64) Gebauer, D.; Cölfen, H. Prenucleation clusters and non-classical nucleation. *Nano Today* **2011**, *6*, 564−584.
(65) Arulanandam, S.; Li, D. Liquid transport in rectangular microchannels by electroosmotic pumping. *Colloids Surf., A* **2000**, *161*, 89−102.
(66) Aslan, M.; Zeiger, M.; Jäckel, N.; Grobelsek, I.; Weingarth, D.; Presser, V. Improved capacitive deionization performance of mixed hydrophobic/hydrophilic activated carbon electrodes. *J. Phys.: Condens. Matter* **2016**, *28*, No. 114003.
(67) Guyes, E. N.; Shocron, A. N.; Simanovski, A.; Biesheuvel, P.; Suss, M. E. A one-dimensional model for water desalination by flow-through electrode capacitive deionization. *Desalination* **2017**, *415*, 8−13.
(68) Wang, L.; Lin, S. Membrane capacitive deionization with constant current vs constant voltage charging: which is better? *Environ. Sci. Technol.* **2018**, *52*, 4051−4060.
(69) Bazant, M. Z.; Thornton, K.; Ajdari, A. Diffuse-charge dynamics in electrochemical systems. *Phys. Rev. E* **2004**, *70*, No. 021506.
(70) Atlas, I.; Ramon, G. Z. Periodic energy conversion in an electric-double-layer capacitor. *J. Colloid Interface Sci.* **2018**, *530*, 675−685.
(71) Amrei, S. H.; Bukosky, S. C.; Rader, S. P.; Ristenpart, W. D.; Miller, G. H. Oscillating Electric Fields in Liquids Create a Long-Range Steady Field. *Phys. Rev. Lett.* **2018**, *121*, No. 185504.
(72) Park, J.-S.; Choi, J.-H.; Woo, J.-J.; Moon, S.-H. An electrical impedance spectroscopic (EIS) study on transport characteristics of ion-exchange membrane systems. *J. Colloid Interface Sci.* **2006**, *300*, 655−662.


https://dx.doi.org/10.1021/acs.est.9b07806
*Environ. Sci. Technol.* XXXX, XXX, XXX−XXX